SCIENCE CHINA
Chemistry

• ARTICLES •
• SPECIAL ISSUE • Organic photovoltaics

February 2015 Vol.58 No.2: 294–300
doi: 10.1007/s11426-014-5221-9

Dithienocarbazole- and benzothiadiazole-based donor-acceptor conjugated polymers for bulk heterojunction polymer solar cells

Ziqing Rong[1,2], Yunfeng Deng[1,2], Zhiyuan Xie[1], Yanhou Geng[1*] & Fosong Wang[1]

[1]*State Key Laboratory of Polymer Physics and Chemistry, Changchun Institute of Applied Chemistry, Chinese Academy of Sciences, Changchun 130022, China*
[2]*University of Chinese Academy of Sciences, Beijing 100049, China*

Received July 24, 2014; accepted August 13, 2014; published online December 29, 2014

Donor-acceptor (D-A)-conjugated polymers P(BT-C1) and P(BT-C2), with dithieno[2,3-*b*;7,6-*b*]carbazole (C1) or dithieno[3,2-*b*;6,7-*b*]carbazole (C2) as D-unit and benzothiadiazole (BT) as A-unit, were synthesized. The optical bandgaps of the polymers are similar (1.84 and 1.88 eV, respectively). The structures of donor units noticeably influence the energy levels and backbone curvature of the polymers. P(BT-C1) shows a large backbone curvature; its highest occupied molecular orbital (HOMO) energy level is −5.18 eV, whereas P(BT-C2) displays a pseudo-straight backbone and has a HOMO energy level of −5.37 eV. The hole mobilities of the polymers without thermal annealing are 1.9×10^{-3} and 2.7×10^{-3} cm^2 V^{-1} s^{-1} for P(BT-C1) and P(BT-C2), respectively, as measured by organic thin-film transistors (OTFTs). Polymer solar cells using P(BT-C1) and P(BT-C2) as the donor and phenyl-C_{71}-butyric acid methyl ester ($PC_{71}BM$) as the acceptor were fabricated. Power conversion efficiencies (PCEs) of 4.9% and 5.0% were achieved for P(BT-C1) and P(BT-C2), respectively. The devices based on P(BT-C2) exhibited a higher V_{oc} due to the deeper HOMO level of the polymer, which led to a slightly higher PCE.

conjugated polymer, dithienocarbazole, benzothiadiazole, polymer solar cells, power conversion efficiency

1 Introduction

Bulk heterojunction (BHJ) polymer solar cells (PSCs) have become an excellent choice for clean and renewable energy resources for their advantages such as easy fabrication of large-area and flexible devices, low fabrication cost, and materials tunability [1–8]. In the past several years, the power conversion efficiency (PCE) of BHJ PSCs has been improved through the design of new materials and the exploration of novel device architectures [9–19]. To date, maximum PCEs of 9.4% and 10.6% have been respectively demonstrated for single-junction [20] and tandem devices [21].

Vast numbers of semiconducting polymers have been developed and applied in BHJ PSC devices. Due to their high mobilities, appropriate HOMO energy levels, and narrow bandgaps, which are required properties for the fabrication of high-performance photovoltaic devices [3–6], donor-acceptor (D-A)-conjugated polymers have become the most successful donor materials. Of those, D-A conjugated polymers based on carbazole and 4,7-bis(thiophen-2-yl)-benzo[*c*][1,2,5]thiadiazole derivatives, such as poly[*N*-9′-heptadecanyl-2,7-carbazole-*alt*-5,5-(4′,7′-di-2-thienyl-2′,1′,3′-benzothiadiazole)] (PCDTBT) and poly(2-(5-(5,6-bis(octyloxy)-4-(thiophen-2-yl)benzo[*c*][1,2,5]thiadiazol-7-yl)thiophen-2-yl)-9-octyl-9*H*-carbazole) (HXS-1), have attracted intense attention [22–28]; PCE has surpassed 7% after the device fabrication condition was optimized [29,30]. Because polyaromatics generally have rigid and planar configurations, incorporating a polyaromatic unit into the backbones of conjugated polymers can make the π-electron delocalization more effective. This in turn leads to a reduced optical bandgap and a red-shifted absorption spectrum [31–34]. In

*Corresponding author (email: yhgeng@ciac.ac.cn)

addition, molecules with coplanar and rigid structure usually have smaller reorganization energy, which is beneficial for achieving high charge-carrier mobility [35–39]. Recently, we reported two novel polyaromatics based on carbazole: dithieno[2,3-*b*;7,6-*b*]carbazole (C1) and dithieno[3,2-*b*; 6,7-*b*]carbazole (C2). D-A-conjugated polymers with C1 or C2 as D units and diketopyrrolopyrrole (DPP) or isoindigo (IID) as A units exhibited field-effect mobilities up to 1.36 $cm^2\ V^{-1}s^{-1}$ and PCEs up to 8.2% [40–44]. Herein we report two novel polymers P(BT-C1) and P(BT-C2) (Figure 1) by replacing the carbazole unit in HXS-1 [26] with C1 or C2. In order to ensure solubility, dodecyloxy instead of octyloxy was used in the benzo[*c*][1,2,5]thiadiazole (BT) unit. The photophysical, semiconducting, and photovoltaic properties of the resulting polymers were studied in detail.

2 Results and discussion

2.1 Synthesis of the polymers and their thermal properties

Synthetic routes of the monomers and polymers are depicted in Scheme S1(see the Supporting Information online). Number-average molecular weight (M_n) and polydispersity index (PDI) were 45.0 kDa and 3.97 for P(BT-C1) and 47.9 kDa and 2.60 for P(BT-C2), as measured by gel permeation chromatography (GPC) at 150 °C with 1,2,4-trichlorobenzene as eluent and polystyrene as standard. Both polymers showed good solubility in chlorinated organic solvents, such as chlorobenzene and *o*-dichlorobenzene (*o*-DCB), and were thermally stable with 5% weight-loss temperatures (T_d) above 300 °C as revealed by thermogravimetric analysis (TGA) (Figure S1). Two decomposition steps were observed in TGA curves, which can be attributed to the decomposition of the alkyl chains in the carbzole and BT moieties. No obvious thermal transitions were observed in their differential scanning calorimetry (DSC) curves (Figure S2), which indicated that both polymers are amorphous. This characteristic of the polymers was also confirmed by X-ray diffraction (XRD) studies. As shown in Figure S3, no diffraction peaks were observed in the film XRD patterns.

2.2 Optical and electrochemical properties

Figure 2 shows solution and film UV-Vis absorption spectra of P(BT-C1) and P(BT-C2). Both polymers have two distinct absorption bands in both solution and film states. The first absorption band is ascribed to π-π* transition and the second one, in the low-energy region, is attributed to intramolecular charge transfer (ICT) interaction between D and A building blocks [45]. In solution, the absorption maxima are 404 and 562 nm for P(BT-C1) and 425 and 568 nm for P(BT-C2). From solution to film, the absorption maxima at short wavelengths exhibited a small red-shift (⩽5 nm), while those at long wavelengths displayed a rather large red-shift of 14 nm for P(BT-C1) and 10 nm for P(BT-C2). This phenomenon, which is quite similar to what has been observed in many other conjugated polymers, is ascribed to the enhanced molecular aggregation or interchain interaction in solid state [46]. The most notable difference between the absorption spectra of P(BT-C1) and P(BT-C2) is the relative intensity of two absorption bands. Compared to P(BT-C1), P(BT-C2) has a higher absorption intensity in the long wavelength region but a lower absorption intensity in the short wavelength region, which implies that a pseudo-straight backbone conformation may lead to strong ICT interaction between the D and A units by sacrificing the π-π* transition. Absorption coefficients at the long wavelength region were determined to be around 3.5×10^4 for P(BT-C1) and and 4.5×10^4 cm^{-1} for P(BT-C2). The absorption onset of P(BT-C1) was slightly red-shifted relative to that of P(BT-C2); therefore, P(BT-C1) has a smaller optical bandgap (1.84 eV vs. 1.88 eV for P(BT-C2)). Compared to polymer HXS-1, which incorporates octyloxy groups on the electron-deficient BT unit and a straight *N*-octyl chain on the carbazole unit developed by Bo, the absorption onsets of our polymers showed ~50 nm red-shift [26] owing to the electron-richer characteristic than carbazole of the dithienocarbazole units.

To determine the highest occupied molecular orbital (HOMO) and the lowest unoccupied molecular orbital (LUMO) energy levels of the polymers, film cyclic voltammograms (CVs) were recorded. As shown in Figure 3, both polymers exhibited reversible redox behavior at either positive or negative potential region. The HOMO/LUMO energy levels were −5.18 eV/−3.18 eV for P(BT-C1) and −5.37 eV/−3.01 eV for P(BT-C2) (Table 1), as determined from the oxidation- (E_{on}^{ox}) and reduction (E_{on}^{re})-onset potentials in the CV curves according to the equations HOMO =−(4.80+E_{on}^{ox}) eV and LUMO=−(4.80+E_{on}^{re}) eV. Interestingly, the HOMO level of P(BT-C2) is deeper than that of P(BT-C1), even though their molecular structures are almost the same except for the positions of the S atoms in the dithienocarbazole units.

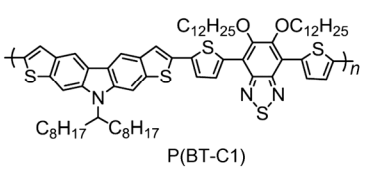

P(BT-C1)

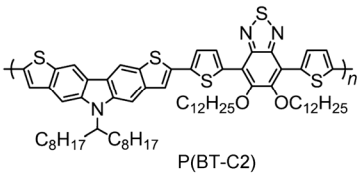

P(BT-C2)

Figure 1 Chemical structures of the polymers P(BT-C1) and P(BT-C2).

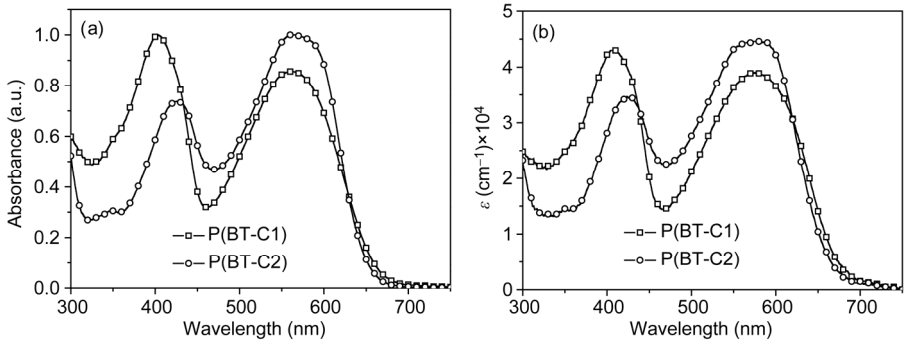

Figure 2 Solution (a, 10^{-5} mol L^{-1} of the repeating units in *o*-DCB) and film (b) UV-Vis absorption spectra of the polymers. The films were prepared by spin-casting *o*-DCB solutions (5 mg mL^{-1}) onto quartz substrates.

Table 1 Number-average molecular weights (M_ns), polydispersity indices (PDIs), thermal decomposition temperatures (T_ds), and optical and electrochemical properties of the polymers

Polymer	M_n (kDa)	PDI	T_d (°C) [a]	λ_{max} (nm)		HOMO (eV) [c]	LUMO (eV) [c]	E_g^{opt} (eV) [d]
				Solution [b]	film			
P(BT-C1)	45.0	3.97	322	404, 562	409, 576	–5.18	–3.18	1.84
P(BT-C2)	47.9	2.60	325	425, 568	427, 578	–5.37	–3.01	1.88

a) Reported as the temperature with 5% weight loss. b) Measured in *o*-DCB (concentration: 10^{-5} mol/L of the repeating unit). c) HOMO and LUMO energy levels were calculated according to HOMO=–(4.80+E_{on}^{ox}) eV and LUMO=–(4.80+E_{on}^{re}) eV, in which E_{on}^{ox} and E_{on}^{re} are the oxidation and reduction onset potentials versus Fc/Fc^+, respectively. d) Optical bandgap (E_g^{opt}) was calculated from the film absorption onset.

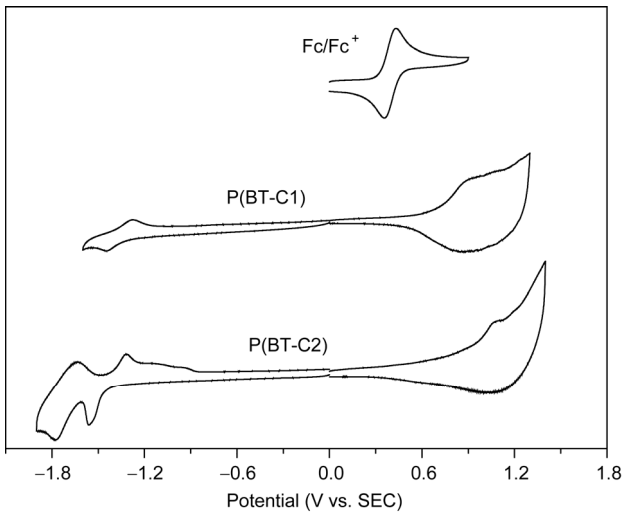

Figure 3 Cyclic voltammograms (CVs) of the polymers. The films were prepared by spin-casting *o*-DCB solutions with a concentration of 5 mg mL^{-1} onto the electrode. CV of ferrocene (Fc) was also included for comparison.

In order to understand the optical and electrochemical properties discussed above, we performed density functional theory (DFT) computations on conjugated segments containing three repeating units, using Gaussian 09 with a hybrid B3LYP correlation functional and a split valence 6–31 G basis set. Longer alkyl side-chains were replaced by methyl groups to simplify the calculations. As shown in Figure 4, two polymers presented distinct backbone conformations. P(BT-C1) showed a large backbone curvature, while P(BT-C2) possessed a pseudo-straight backbone conformation. For both polymers, the HOMO wave function delocalizes over more than two repeating units, whereas the LUMO wave function mainly localizes on the BT moieties. This is typical for D-A-type conjugated polymers [47,48]. However, the HOMO of P(BT-C2) is slightly less delocalized than that of P(BT-C1), which may be responsible for the low-lying HOMO of P(BT-C2) [48]. The calculated HOMO energy levels for P(BT-C1) and P(BT-C2) of –4.86 and –4.96 eV, respectively, are close to the values obtained from CV measurements.

2.3 Charge transport properties

Organic thin-film transistors (OTFTs) with a bottom-gate and top-contact configuration were fabricated to investigate the charge-carrier transport properties of P(BT-C1) and P(BT-C2). Fabrication and measurement of the devices are outlined in the Supporting Information online. Both polymers exhibited typical *p*-type characteristics (Table S1 and Figure 5). The hole mobilities of the devices based on pristine films are 1.9×10^{-3} and 2.7×10^{-3} cm^2 V^{-1} s^{-1} for P(BT-C1) and P(BT-C2), respectively. After thermal annealing, no improvement was observed in the mobility of P(BT-C1). However, the mobility of P(BT-C2) was enhanced to 5.4×10^{-3} cm^2 V^{-1} s^{-1} after the film was thermally annealed at 200 °C for 20 min. This different behavior can be attributed to the different backbone conformations of the two

polymers. Although the polymers are amorphous, P(BT-C2) has a relatively straight backbone and may be subject to reorganization upon annealing for the formation of a film that comprises more closely-packed conjugated chains. In contrast, the large backbone curvature of P(BT-C1) may impede this process [49,50]. The mobility of P(BT-C1) was in the same magnitude as that of the polymers based on DPP, IID, and thienopyrroledione (TPD). However, the mobility of P(BT-C2) was much lower than that of the polymers with C2 as the donor unit and DPP, IID, or TPD as the acceptor unit [42].

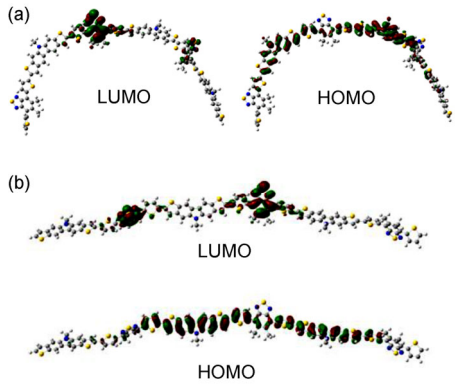

Figure 4 DFT-calculated (B3LYP/6–31G) molecular orbitals of P(BT-C1) (a) and P(BT-C2) (b).

2.4 Photovoltaic properties

The BHJ PSCs were fabricated with a structure of glass/ITO/poly(3,4-ethylenedioxythiophene)/poly(styrene sulfonate) (PEDOT:PSS)/polymer:$PC_{71}BM$/LiF/Al. Details of the fabrication and test conditions are described in the Supporting Information section. The best blending ratio of polymer:$PC_{71}BM$ was 1:4 (*w*/*w*) for both polymers (Tables S2 and S3). Figure 6 displays current density-voltage (*J*-*V*) curves and external quantum efficiency (EQE) profiles of the devices prepared with the optimized blend ratio; the photovoltaic parameters are summarized in Table 2. The devices based on P(BT-C1) demonstrated a maximum PCE of 4.9% with an open-circuit voltage (V_{oc}) of 0.70 V, a short-circuit current density (J_{sc}) of 10.7 mA cm^{-2}, and a fill factor (FF) of 0.65. Devices based on P(BT-C2) had a higher V_{oc} of 0.79 V, which is in agreement with its deeper HOMO energy level. The PCE reached 5.0% with a J_{sc} of 10.3 mA cm^{-2} and a FF of 0.62. This device performance is largely comparable to that of HXS-1 [26] but lower than that of the polymer based on C2 and IID [44]. We expect further

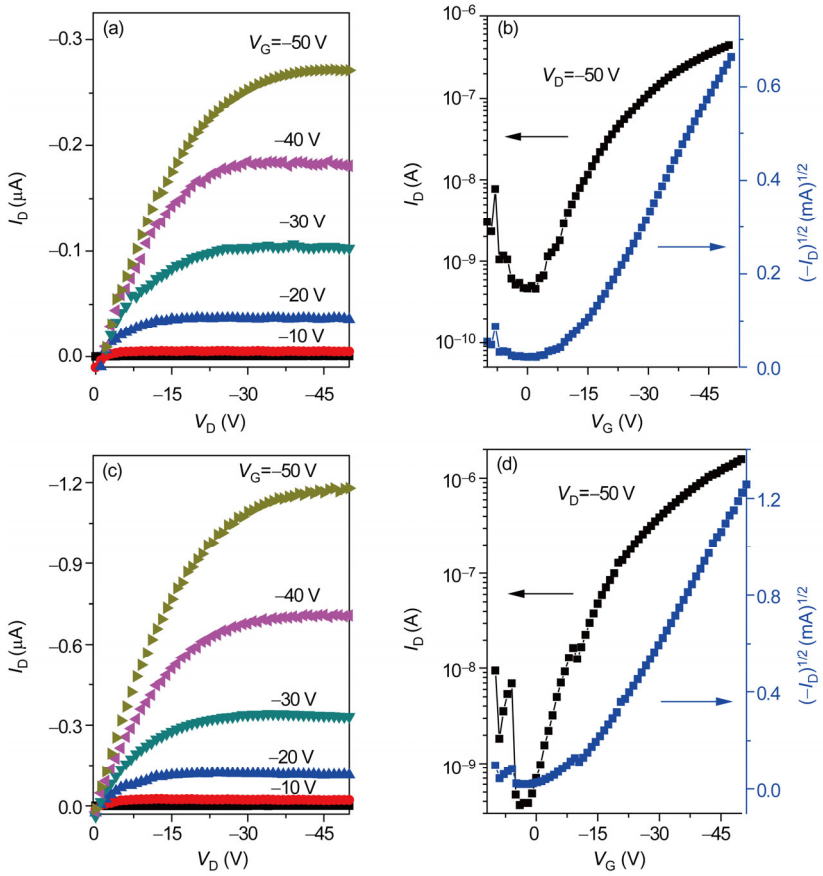

Figure 5 Typical output (a and c) and transfer (b and d) characteristics of OTFTs based on P(BT-C1) (a and b) and P(BT-C2) (c and d). The films were pristine for P(BT-C1) and thermally annealed at 200 °C for 20 min for P(BT-C2).

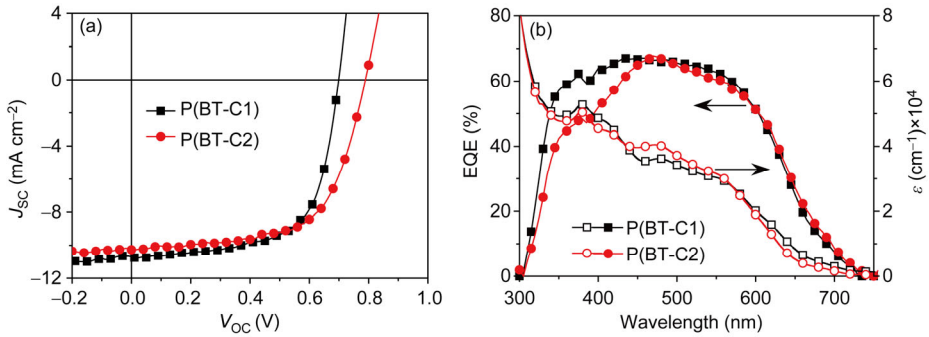

Figure 6 *J-V* characteristics of PSCs based on polymer:$PC_{71}BM$ [1:4 (*w*/*w*)] under AM 1.5G illumination at 100 mW cm^{-2} (a), and EQE profiles of the PSCs and absorption spectra of polymer:$PC_{71}BM$ [1:4 (*w*/*w*)] films (b).

improvement upon optimizing device-fabrication conditions [26–28,30]. As shown in the external quantum efficiency (EQE) profiles (Figure 6(b)), the devices based on both polymers showed a photoresponse range of 300–720 nm, which largely matched the film-absorption spectra of polymer:$PC_{71}BM$ blends; the highest EQE value reached 65%. The slightly higher J_{sc} of the devices based on P(BT-C1) is attributed to the higher EQE, which was in the range of 350–450 nm. The reason for this difference remains unclear, however. The J_{sc} values calculated from the EQE (Table 2) were consistent with the measured data (error range ~3%), which proves the accuracy of these measurements.

The film morphology of polymer:$PC_{71}BM$ blends were studied by atomic force microscopy (AFM) in tapping mode. As shown in Figure 7, both blend films were very smooth and uniform, and possessed a nanoscale phase separation although no additive was used. This behavior is different from HXS-1:$PC_{71}BM$, for which the additive 1,8-diiodooctane was used in order to attain appropriate film morphology [26–28]. Compared to the film of P(BT-C2):$PC_{71}BM$, the film of P(BT-C1):$PC_{71}BM$ had a more obvious phase separation and exhibited a fiber-like morphology. This difference in film morphology may be responsible for the slightly higher J_{sc} and FF of the devices based on P(BT-C1), although this polymer exhibited relatively low mobility and absorption coefficients at the long wavelength region.

Table 2 Device performance of the PSCs under AM 1.5G illumination at 100 mW cm^{-2} a)

Polymer	V_{oc} (V)	J_{sc} (mA cm^{-2})	J_{sc} (mA cm^{-2}) b)	FF	PCE (%) c)
P(BT-C1)	0.70	10.7	10.3	0.65	4.9(4.6)
P(BT-C2)	0.79	10.3	10.0	0.62	5.0(4.9)

a) Polymer:$PC_{71}BM$=1:4 (*w*/*w*); the thickness of the blend films is about 90 nm. b) The values are estimated from EQE profiles. c) The values in parentheses are the average PCEs.

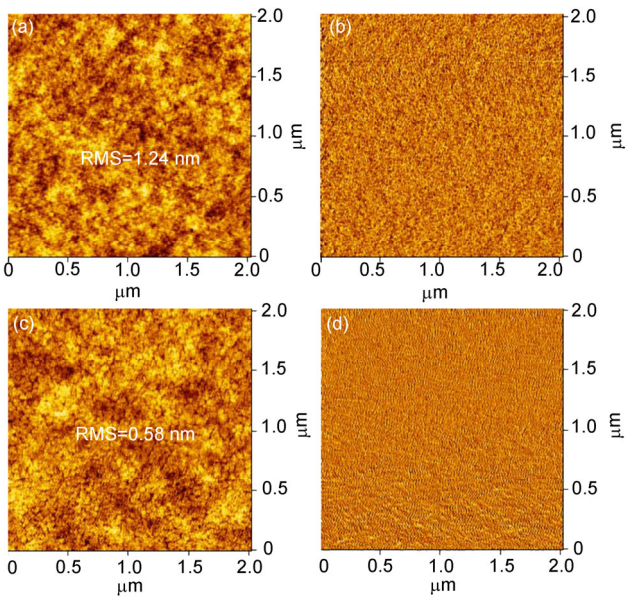

Figure 7 AFM height (a, c) and phase (b, d) images of P(BT-C1):$PC_{71}BM$ (1:4, *w*/*w*) (a, b) and P(BT-C2):$PC_{71}BM$ (1:4, *w*/*w*) (c, d) blend films.

3 Conclusions

We synthesized and characterized two novel D-A-conjugated polymers, P(BT-C1) and P(BT-C2), based on dithienocarbazoles and benzothiadiazole, respectively. The structures of the donor units (C1 and C2) had a noticeable impact on the properties of the polymers. The two polymers have distinct chain conformations and different HOMO levels. Compared to P(BT-C1), which displays a large backbone curvature, the polymer based on C2 (P(BT-C2)) has a pseudo-straight backbone and lower HOMO level, which lead to a higher charge-carrier mobility measured by OTFT and a higher V_{oc} for BHJ PSCs with $PC_{71}BM$ as the electron acceptor. PCEs of 4.9% and 5.0% were demonstrated for P(BT-C1) and P(BT-C2), respectively. Our research reveals that dithienocarbazole units are promising building blocks for D-A-conjugated polymers that are applicable to high-efficiency PSCs.

Supporting information

The supporting information is available online at chem.scichina.com and link.springer.com/journal/11426. The supporting materials are published as submitted, without typesetting or editing. The responsibility for scientific accuracy and content remains entirely with the authors.

This work was financially supported by the National Basic Research Program of China (2014CB643504), the National Natural Science Foundation of China (51273193), and the Strategic Priority Research Program of the Chinese Academy of Sciences (XDB12010300).

1 Cao WR, Xue JG. Recent progress in organic photovoltaics: device architecture and optical design. *Energy Environ Sci*, 2014, 7: 2123–2144
2 Brabec CJ, Gowrisanker S, Halls JJM, Laird D, Jia SJ, Williams SP. Polymer-fullerene bulk-heterojunction solar cells. *Adv Mater*, 2010, 22: 3839–3856
3 Li YF. Molecular design of photovoltaic materials for polymer solar cells: toward suitable electronic energy levels and broad absorption. *Acc Chem Res*, 2012, 45: 723–733
4 Li G, Zhu R, Yang Y. Polymer solar cells. *Nat Photonics*, 2012, 6: 153–161
5 Zhou HX, Yang LQ, You W. Rational design of high performance conjugated polymers for organic solar cells. *Macromolecules*, 2012, 45: 607–632
6 Zhang ZG, Wang JZ. Structures and properties of conjugated donor–acceptor copolymers for solar cell applications. *J Mater Chem*, 2012, 22: 4178–4187
7 Cheng YJ, Yang SH, Hsu CS. Synthesis of conjugated polymers for organic solar cell applications. *Chem Rev*, 2009, 109: 5868–5923
8 Günes S, Neugebauer H, Sariciftci NS. Conjugated polymer-based organic solar cells. *Chem Rev*, 2007, 107: 1324–1338
9 Chao YH, Jheng JF, Wu JS, Wu KY, Peng HH, Tsai MC, Wang CL, Hsiao YN, Wang CL, Lin CY, Hsu CS. Porphyrin-incorporated 2D D-A polymers with over 8.5% polymer solar cell efficiency. *Adv Mater*, 2014, 26: 5205-5210
10 Zhang MJ, Guo X, Ma W, Zhang SQ, Huo LJ, Ade H, Hou JH. An easy and effective method to modulate molecular energy level of the polymer based on benzodithiophene for the application in polymer solar cells. *Adv Mater*, 2014, 26: 2089–2095
11 Yusoff ARM, Lee SJ, Kim HP, Shneider FK, Silva WJ, Jang J. 8.91% power conversion efficiency for polymer tandem solar cells. *Adv Funct Mater*, 2014, 24: 2240–2247
12 Jiang JM, Lin HK, Lin YC, Chen HC, Lan SC, Chang CK, Wei KH. Side chain structure affects the photovoltaic performance of two-dimensional conjugated polymers. *Macromolecules*, 2014, 47: 70–78
13 Li K, Li ZJ, Feng K, Xu XP, Wang LY, Peng Q. Development of large band-gap conjugated copolymers for efficient regular single and tandem organic solar cells. *J Am Chem Soc*, 2013, 135: 13549–13557
14 Zhang MJ, Gu Y, Guo X, Liu F, Zhang SQ, Huo LJ, Russell TP, Hou JH. Efficient polymer solar cells based on benzothiadiazole and alkylphenyl substituted benzodithiophene with a power conversion efficiency over 8%. *Adv Mater*, 2013, 25: 4944–4949
15 Wang N, Chen Z, Wei W, Jiang ZH. Fluorinated benzothiadiazole-based conjugated polymers for high-performance polymer solar cells without any processing additives or post-treatments. *J Am Chem Soc*, 2013, 135: 17060 –17068
16 Guo XG, Zhou NJ, Lou SJ, Smith J, Tice DB, Hennek JW, Ortiz RP, Navarrete JTL, Li SY, Strzalka J, Chen LX, Chang RPH, Facchetti A, Marks TJ. Polymer solar cells with enhanced fill factors. *Nat Photonics*, 2013, 7: 825–833
17 Son HJ, Lu LY, Chen W, Xu T, Zheng TY, Carsten B, Strzalka J, Darling SB, Chen LX, Yu LP. Synthesis and photovoltaic effect in dithieno[2,3-d:2′,3′-d′]benzo[1,2-b:4,5-b′]dithiophene-based conjugated polymers. *Adv Mater*, 2013, 25: 838–843
18 Li XH, Choy WCH, Huo LJ, Xie FX, Sha WEI, Ding BF, Guo X, Li YF, Hou JH, You JB, Yang Y. Dual plasmonic nanostructures for high performance inverted organic solar cells. *Adv Mater*, 2012, 24: 3046–3052
19 Chu TY, Lu JP, Beaupré S, Zhang YG, Pouliot JR, Zhou JY, Najari A, Leclerc M, Tao Y. Effects of the molecular weight and the side-chain length on the photovoltaic performance of dithienosilole/thienopyrrolodione copolymers. *Adv Funct Mater*, 2012, 22: 2345–2351
20 Ye L, Zhang SQ, Zhao WC, Yao HF, Hou JH. Highly efficient 2D-conjugated benzodithiophene-based photovoltaic polymer with linear alkylthio side chain. *Chem Mater*, 2014, 26: 3603–3605
21 You JB, Dou LT, Yoshimura K, Kato T, Ohya K, Moriarty T, Emery K, Chen CC, Gao J, Li G, Yang Y. A polymer tandem solar cell with 10.6% power conversion efficiency. *Nat Commun*, 2013, 4: 1446–1455
22 Blouin N, Michaud A, Leclerc M. A low-bandgap poly(2,7-carbazole) derivative for use in high-performance solar cells. *Adv Mater*, 2007, 19: 2295–2300
23 Liu J, Shao SY, Fang G, Meng B, Xie ZY, Wang LX. High-efficiency inverted polymer solar cells with transparent and work-function tunable MoO_3-Al composite film as cathode buffer layer. *Adv Mater*, 2012, 24: 2774–2779
24 Liu J, Shao SY, Meng B, Fang G, Xie ZY, Wang LX, Li XL. Enhancement of inverted polymer solar cells with solution-processed ZnO-TiO_x composite as cathode buffer layer. *Appl Phys Lett*, 2012, 100: 213906
25 Yang SP, Zhang Y, Jiang T, Sun XF, Lu CQ, Li G, Li XW, Fu GS. Enhancing the power conversion efficiency of PCDTBT:PC_{71}BM polymer solar cells using a mixture of solvents. *Chin Sci Bull*, 2014, 59: 297–300
26 Qin RP, Li WW, Li CH, Du C, Veit C, Schleiermacher HF, Andersson M, Bo ZS, Liu ZP, Inganäs O, Wuerfel U, Zhang FL. A planar copolymer for high efficiency polymer solar cells. *J Am Chem Soc*, 2009, 131: 14612–14613
27 Qin RP, Jiang YR, Ma H, Yang L, Liu HZ, Chang FG. Carbazoles on same main chain for polymer solar cells. *J Appl Polym Sci*, 2013, 129: 2671–2678
28 Ding P, Chu CC, Zou YP, Xiao DQ, Pan CY, Hsu CS. New low bandgap conjugated polymer derived from 2,7-carbazole and 5, 6-bis(octyloxy)-4,7-di(thiophen-2-yl) benzothiadiazole: synthesis and photovoltaic properties. *J Appl Polym Sci*, 2012, 123: 99–107
29 Zhang Y, Zhou HQ, Seifter J, Ying L, Mikhailovsky A, Heeger AJ, Bazan GC, Nguyen TQ. Molecular doping enhances photoconductivity in polymer bulk heterojunction solar cells. *Adv Mater*, 2013, 25: 7038–7044
30 Meng B, Fang G, Fu YY, Xie ZY, Wang LX. Fine tuning of the PCDTBT-OR:PC_{71}BM blend nanoscale phase separation via selective solvent annealing toward high-performance polymer photovoltaics. *Nanotechnology*, 2013, 24: 484004
31 Chang CY, Cheng YJ, Hung SH, Wu JS, Kao WS, Lee CH, Hsu CS. Combination of molecular, morphological, and interfacial engineering to achieve highly efficient and stable plastic solar cells. *Adv Mater*, 2012, 24: 549–553
32 Wu JS, Cheng YJ, Lin TY, Chang CY, Shih PI, Hsu CS. Dithienocarbazole-based ladder-type heptacyclic arenes with silicon, carbon, and nitrogen bridges: synthesis, molecular properties, field-effect transistors, and photovoltaic applications. *Adv Funct Mater*, 2012, 22: 1711–1722
33 Jacob J, Sax S, Piok T, List EJW, Grimsdale AC, Müllen K. Ladder-type pentaphenylenes and their polymers: efficient blue-light emitters and electron-accepting materials via a common intermediate. *J Am Chem Soc*, 2004, 126: 6987–6995
34 Mishra AK, Graf M, Grasse F, Jacob J, List EJW, Müllen K. Blue-emitting carbon- and nitrogen-bridged poly(ladder-type tetraphenylene)s. *Chem Mater*, 2006, 18: 2879–2885
35 Cheng YJ, Ho YJ, Chen CH, Kao WS, Wu CE, Hsu SL, Hsu CS. Synthesis, photophysical and photovoltaic properties of conjugated

polymers containing fused donor-acceptor dithienopyrrolobenzothiadiazole and dithienopyrroloquinoxaline arenes. *Macromolecules*, 2012, 45: 2690–2698
36 Chen CH, Cheng YJ, Chang CY, Hsu CS. Donor-acceptor random copolymers based on a ladder-type nonacyclic unit: synthesis, characterization, and photovoltaic applications. *Macromolecules*, 2011, 44: 8415–8424
37 Ando SJ, Nishida JI, Tada H, Inoue YJ, Tokito S, Yamashita Y. High performance n-type organic field-effect transistors based on π-elec tronic systems with trifluoromethylphenyl groups. *J Am Chem Soc*, 2005, 127: 5336–5337
38 Liang YY, Wu Y, Feng DQ, Tsai ST, Son HJ, Li G, Yu LP. Development of new semiconducting polymers for high performance solar cells. *J Am Chem Soc*, 2009, 131: 56–57
39 Koster LJA, Shaheen SE, Hummelen JC. Pathways to a new efficiency regime for organic solar cells. *Adv Energy Mater*, 2012, 2: 1246–1253
40 Chen YG, Tian HK, Yan DH, Geng YH, Wang FS. Conjugated polymers based on a S- and N-containing heteroarene: synthesis, characterization, and semiconducting properties. *Macromolecules*, 2011, 44: 5178–5185
41 Chen YG, Liu CF, Tian HK, Bao C, Zhang XJ, Yan DH, Geng YH, Wang FS. Novel conjugated polymers based on dithieno[3,2-b: 6,7-b]carbazole for solution processed thin-film transistors. *Macromol Rapid Commun*, 2012, 33: 1759–1764
42 Deng YF, Chen YG, Zhang XJ, Tian HK, Bao C, Yan DH, Geng YH, Wang FS. Donor-acceptor conjugated polymers with dithienocarbazoles as donor units: effect of structure on semiconducting properties. *Macromolecules*, 2012, 45: 8621–8627
43 Deng YF, Chen YG, Liu J, Liu LH, Tian HK, Xie ZY, Geng YH, Wang FS. Low-band-gap conjugated polymers of dithieno [2,3-b:7, 6-b]carbazole and diketopyrrolopyrrole: effect of the alkyl side chain on photovoltaic properties. *ACS Appl Mater Inter*, 2013, 5: 5741–5747
44 Deng YF, Liu J, Wang JT, Liu LH, Li WL, Tian HK, Zhang XJ, Xie ZY, Geng YH, Wang FS. Dithienocarbazole and isoindigo based amorphous low bandgap conjugated polymers for efficient polymer solar cells. *Adv Mater*, 2014, 26: 471–476
45 Jespersen KG, Beenken WJD, Zaushitsyn Y, Yartsev A, Andersson M, Pullerits T, Sundström V. The electronic states of polyfluorene copolymers with alternating donor-acceptor units. *J Chem Phys*, 2004, 121: 12613–12617
46 Peet J, Cho NS, Lee SK, Bazan GC. Transition from solution to the solid state in polymer solar cells cast from mixed solvents. *Macromolecules*, 2008, 41: 8655–8659
47 Kim JG, Yun MH, Kim GH, Lee JH, Lee SM, Ko SJ, Kim YH, Dutta GK, Moon MJ, Park SY, Kim DS, Kim JY, Yang CD. Synthesis of PCDTBT-based fluorinated polymers for high open-circuit voltage in organic photovoltaics: towards an understanding of relationships between polymer energy levels engineering and ideal morphology control. *ACS Appl Mater Inter*, 2014, 6: 7523–7534
48 Casey A, Ashraf RS, Fei ZP, Heeney M. Thioalkyl-substituted benzothiadiazole acceptors: copolymerization with carbazole affords polymers with large stokes shifts and high solar cell voltages. *Macromolecules*, 2014, 47: 2279–2288
49 Lee WH, Kim GH, Ko SJ, Yum SJ, Hwang SG, Cho S, Shin YH, Kim JY, Woo HY. Semicrystalline D-A copolymers with different chain curvature for applications in polymer optoelectronic devices. *Macromolecules*, 2014, 47: 1604–1612
50 Zuo GZ, Li ZJ, Zhang MJ, Guo X, Wu Y, Zhang SQ, Peng B, Wei W, Hou JH. Influence of the backbone conformation of conjugated polymers on morphology and photovoltaic properties. *Polym Chem*, 2014, 5: 1976–1981